Identification of Ultrasonic Echolucent Carotid Plaques Using Discrete Fréchet Distance Between Bimodal Gamma Distributions

Xiaowei Huang, Yanling Zhang, Long Meng, Ming Qian, *Member, IEEE*, Kelvin Kian Loong Wong, Derek Abbott, *Fellow, IEEE*, Rongqin Zheng, Hairong Zheng, *Senior Member, IEEE*, and Lili Niu

Abstract*—*Objective: **Echolucent carotid plaques are associated with acute cardiovascular and cerebrovascular events (ACCEs) in atherosclerotic patients. The aim of this study was to develop a computer-aided method for identifying echolucent plaques.** ***Methods:*** **A total of 315 ultrasound images of carotid plaques (105 echo-rich, 105 intermediate, and 105 echolucent) collected from 153 patients were included in this study. A bimodal gamma distribution was proposed to model the pixel statistics in the gray scale images of plaques. The discrete Fréchet distance features (DFDFs) of each plaque were extracted based on the statistical model. The most discriminative features (MDFs) were obtained from DFDFs by the linear discriminant analysis, and a k-nearest-neighbor classifier was implemented for classification of different types of plaques.** ***Results:*** **The classification accuracy of the three types of plaques using MDFs can reach 77.46%. When a receiver operating characteristics curve was produced to identify echolucent plaques, the area under the curve was 0.831.** ***Conclusion:*** **Our results indicate potential feasibility of the method for identifying echolucent plaques based on DFDFs.** ***Significance:*** **Our method may potentially improve the ability of noninvasive ultrasonic examination in risk prediction of ACCEs for patients with plaques.**

***Index Terms*—Bimodal gamma distribution, carotid plaque, discrete Fréchet distance, ultrasound imaging.**

Manuscript received August 8, 2016; revised December 22, 2016 and February 15, 2017; accepted February 21, 2017. Date of publication March 1, 2017; date of current version April 19, 2018. The work was supported by 973 Program (Grant No. 2015CB755500) and National Science Foundation Grants (NSFC Grant Nos. 81527901, 11325420, 11574341, 11674347), Shenzhen Basic Science Research (JCYJ20160429190550139, JCYJ20160429184552717). *(Corresponding author: Hairong Zheng.)*

X. Huang is with the Shenzhen Institutes of Advanced Technology, Chinese Academy of Sciences, and Shenzhen College of Advanced Technology, University of Chinese Academy of Sciences.

Y. Zhang and R. Zheng are with the Department of Ultrasound, Third affiliated hospital, Sun Yat-sen University.

L. Meng and M. Qian are with the Shenzhen Institutes of Advanced Technology, Chinese Academy of Sciences.

K. K. L. Wong is with the School of Medicine, Western Sydney University.

D. Abbott is with the Centre for Biomedical Engineering, and School of Electrical and Electronic Engineering, University of Adelaide.

*H. Zheng and L. Niu are with the Shenzhen Institutes of Advanced Technology, Chinese Academy of Sciences, Shenzhen 518055, China (e-mail: hr.zheng@siat.ac.cn).

Digital Object Identifier 10.1109/TBME.2017.2676129

I. Introduction

ACUTE cardiovascular and cerebrovascular events (ACCEs) are major causes of disability and premature death worldwide for subjects without obvious symptoms [1], [2]. Plaque echogenicity assessed by B-mode ultrasound has been reported to be associated with cardiovascular and cerebrovascular events in previous studies [3]–[5]. Echolucent plaques have higher lipid and macrophage, signifying a higher risk for ACCEs [6]–[9]. Therefore, we proposed a computer-aided method to identify echolucent plaques, which may potentially improve risk prediction of ACCEs for patients with plaques.

In recent years, the gamma distribution has been widely adopted for modeling gray level distribution in synthetic aperture radar images [10], [11], mammogram images [12], and ultrasound images [13]–[17]. Li *et al.* have reported that the gamma distribution is useful for the statistical modeling of amplitude synthetic aperture radar images [10]. Qin *et al.* have indicated that the gamma distribution is a flexible empirical model for synthetic aperture radar images, and the categories of synthetic aperture radar images can be discriminated using the Kullback–Leibler distance between gamma distributions [11]. Gumaei *et al.* have shown that the gamma distribution is suitable for describing symmetric and non-symmetric mammogram images, and can improve the accuracy of breast cancer detection. Tao *et al.* model cardiac ultrasound images based on four families of distributions (gamma, Weibull, normal, and log-normal), and find that the gamma distribution demonstrate improved performance in fitting the data and a low misclassification rate in classifying blood and tissue [15]. The study of Vegas-Sánchez-Ferrero *et al.* have shown desirable performance of the generalized gamma distribution in characterizing the speckle of blood and myocardial tissue in ultrasonic images [16]. They also propose a plaque characterization method for intravascular ultrasonic images based on the gamma distribution [17]. The unimodal gamma distribution is characterized by two parameters and is useful for describing most of the homogeneous images, but it may be inadequate for modelling images with complex structures [18], [19].The distribution of gray levels in B-mode ultrasound images of carotid plaques is complicated as the plaques have heterogeneous histologic components (e.g. calcifications, lipids, hemorrhages, fibrous tissue etc.) [20]. Thus, a bimodal gamma distribution with five

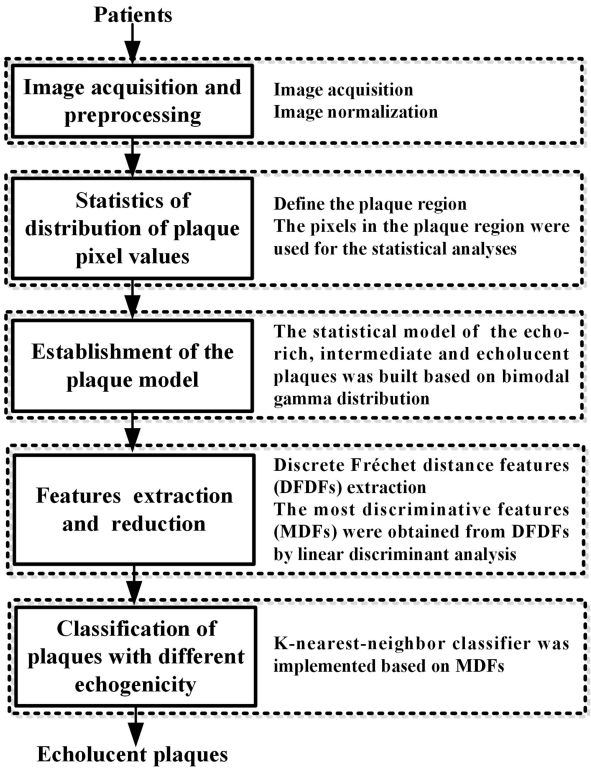

Fig. 1. Flowchart for the classification of echolucent carotid plaques based on the discrete Fréchet distance features.

parameters may be sufficient to describe the ultrasound images of plaques. Shankar *et al.* report 33 ultrasound images of plaques indicating that a bimodal gamma distribution model is effective in modeling hard and soft plaques [13]. However, this is an incomplete scheme for feature extraction and classification of plaques with different echogenicity. According to the criteria of the European carotid plaque study group, the plaques can be classified into echo-rich, intermediate and echolucent plaques [21]. In our study, the bimodal gamma distribution is proposed to model the pixel statistics of the gray scale images of the three different types of plaques. There are three curves representing the echo-rich, intermediate and echolucent plaques in the model. Furthermore, previous studies have indicated that discrete Fréchet distance is feasible for quantitative assessment of the similarity of two curves [22], [23]. The discrete Fréchet distance features (DFDFs) were extracted from the relationship between the cumulative distribution curve of the pixel gray value distribution of each plaque and the three curves in the statistical model, respectively.

Our study aims to develop a computer-aided method based on DFDFs for identifying echolucent plaques, which may potentially improve the ability of ultrasonic examination in risk prediction of ACCEs for patients with carotid plaques. The flowchart of the method is shown in Fig. 1.

II. Materials and Methods

A. Materials

A total of 315 ultrasound images of carotid plaques (105 echo-rich, 105 intermediate and 105 echolucent) collected from 153 subjects were analyzed in our study. The plaques were randomly divided into a training group (70 echo-rich, 70 intermediate and 70 echolucent images) and a test group (35 echo-rich, 35 intermediate and 35 echolucent images). In order to improve reliability of the results, a three-fold cross validation test was performed, and the mean accuracy was taken as the final result.

B. Images Acquisition and Preprocessing

From February 2014 to October 2015, ultrasound carotid plaque images were collected using an Aplio XG (SSA-790A, Toshiba Medical Systems, Japan) equipped with a 5–12 MHz (center frequency is 8 MHz) linear-array transducer (PLT-805AT) and a MyLab90 (Esaote Medical Systems, Italy) equipped with a 4–13 MHz (center frequency is 8 MHz) linear-array transducer (LA523) by a sonographer with five years of experience in vascular imaging. The carotid artery was examined with the head tilted slightly upward in the mid-line position. The transducer was manipulated so that the near and far walls were parallel to the transducer footprint, and the lumen diameter was maximized in the longitudinal plane. All participants provided written informed consent. The study protocol was approved by the Institutional Review Board of the third affiliated hospital of Sun Yat-sen University (Guangzhou, China).

Plaque echogenicity was visually classified into type 1 (echo-rich), type 2 (intermediate) and type 3 (echolucent) according to the criteria of the European carotid plaque study group [21]. The assessment of plaque echogenicity was performed by two sonographers with at least five years experience in vascular imaging, and the controversial plaques were removed. A Cohen's kappa coefficient (κ) was calculated to evaluate the inter-observer agreement. To improve the comparability of the images and the reliability of our results, the images were normalized according to the scheme proposed by Sabetai *et al.* [24]. After normalization, the gray-scale median (GSM) of the blood range from 0 to 5, and the GSM of adventitia range from 185 to 195.

C. Statistics of Gray Value Distribution of Plaque Pixels

The plaque region within each image was manually defined by an experienced vascular sonographer, and the statistic of the gray value distribution of each plaque was obtained. Let x denote pixel value, where $f(x)$ is the probability density function (PDF) of x, and the empirical cumulative distribution function (CDF), $F_{\text{plaque}}(x)$, can be expressed by:

$$F_{\text{plaque}}(x_i) = \frac{\sum_{x=0}^{x_i} f(x)}{\sum_{x=0}^{255} f(x)},\ x_i = 0,\ 1,\ \ldots,\ 254,\ 255. \quad (1)$$

D. Bimodal Gamma Distribution

For a parameter $\alpha > 0$, gamma function $\Gamma(\alpha)$ is defined by:

$$\Gamma(\alpha) = \int_0^{\infty} x^{\alpha-1} e^{-x} dx. \quad (2)$$

A variable x that is gamma-distributed with shape k and scale θ is denoted by $\mathrm{X} \sim \Gamma(\mathrm{k},\ \theta)$. Its PDF is defined as

$$f\ (x;\ k,\ \theta) = \frac{x^{k-1} e^{-\frac{x}{\theta}}}{\theta^k \Gamma(k)},\ x > 0,\ k > 0,\ \theta > 0. \quad (3)$$

The corresponding CDF is calculated by (4). For a bimodal gamma distribution, its PDF and CDF can be expressed by (5) and (6), respectively.

$$F(x_i;\ k,\ \theta) = \int_0^{x_i} f(x;\ k,\ \theta)\,dx = \int_0^{x_i} \frac{x^{k-1}e^{-\frac{x}{\theta}}}{\theta^k \Gamma(k)}dx \quad (4)$$

$$f_{\text{gamma}}(x,\ \beta,\ k_1,\ \theta_1,\ k_2,\ \theta_2) = \beta \frac{x^{k_1-1}e^{-\frac{x}{\theta_1}}}{{\theta_1}^{k_1}\Gamma(k_1)} + (1-\beta)\frac{x^{k_2-1}e^{-\frac{x}{\theta_2}}}{{\theta_2}^{k_2}\Gamma(k_2)} \quad (5)$$

$$F_{\text{gamma}}(x_i,\ \beta,\ k_1,\ \theta_1,\ k_2,\ \theta_2) = \int_0^{x_i}\left[\beta\frac{x^{k_1-1}e^{-\frac{x}{\theta_1}}}{{\theta_1}^{k_1}\Gamma(k_1)} + (1-\beta)\frac{x^{k_2-1}e^{-\frac{x}{\theta_2}}}{{\theta_2}^{k_2}\Gamma(k_2)}\right]dx. \quad (6)$$

E. Statistical Model of Plaques

We investigated the ability of a bimodal gamma distribution in modeling the gray scale distribution of the plaque. There are five parameters (β, k_1, θ_1, k_2 and θ_2) that can be adjusted for curve-fitting implemented between the CDF of the bimodal gamma distribution and the empirical CDF of the plaque. In order to guarantee the reliability of curve-fitting, the parameters were obtained by minimizing the error (all $\varepsilon < 0.05$), given by:

$$\varepsilon = \sum_{x=0}^{255}\left[F_{\text{plaque}}(x) - F_{\text{gamma}}(x)\right]^2 \quad (7)$$

where $\mathrm{F_{plaque}(x)}$ and $\mathrm{F_{gamma}(x)}$ were obtained from (1) and (6), respectively. Further, we proposed a statistical model that can be used for classifying the three types of plaques. The gray value distributions of echo-rich, intermediate and echolucent plaques in the training group were obtained respectively according to the following equation:

$$F_{\text{model}}(x_i) = \frac{\sum_{x=0}^{x_i}\left(f_1(x) + f_2(x) + \cdots + f_{\text{M}}(x)\right)}{\sum_{x=0}^{225}\left(f_1(x) + f_2(x) + \cdots + f_{\text{M}}(x)\right)} \quad (8)$$

where M is the plaque label in the training set, $f_{\text{M}}(x)$ represents the probability of x of Mth plaque. Thus the data used for modeling was obtained. Curve-fitting techniques were performed between the CDF of bimodal gamma distribution and $F_{\text{model}}(x_i)$ in (8). Therefore, a statistical mode $F_{\text{model-gamma}}(x_i)$ were achieved, which included three curves denoting the echo-rich, intermediate and echolucent plaques, respectively.

F. Feature Extraction

1) Discrete Fréchet Distance: Assume a path $Z = \langle z_1, \ldots, z_r\rangle$ of r vertices, a t-walk along Z means Z is partitioned along the path into t disjoint nonempty subpaths $\{Z_j\}_{j=1,\ldots,t}$ such that $Z_j = \langle z_{r_{j-1}+1}, \ldots, z_{r_j}\rangle$ and $0 = r_0 < r_1 < \cdots < r_t = r$. For two paths $A = \langle a_1, \ldots, a_n\rangle$ and $B = \langle b_1, \ldots, b_m\rangle$, a paired walk $W = \{(A_j, B_j)\}$ along A and B is a t-walk $\{A_j\}_{j=1,\ldots,t}$ along A and a t-walk $\{B_j\}_{j=1,\ldots,t}$ along B for some t, such that, for $1 \le j \le t$, $|A_j| = 1$ or $|B_j| = 1$ (i.e., either A_j or B_j contains exactly one vertex). The discrete Fréchet distance between two paths A and B is:

$$\text{dis}_F(A,\ B) = \min_W \max_j \max_{(a,\ b)\in A_j \times B_j} \text{dis}(a,\ b) \quad (9)$$

where dis(a, b) represents the Euclidean distance between two points a and b. In this study, the discrete Fréchet distance was proposed to measure the similarity between CDF of each plaque and the three model curves. The discrete Fréchet distance between two paths $F_{\text{model-gamma}}(x_i)$ or $F_{\text{plaque}}(x)$ is:

$$\text{DFDF} = \text{dis}_F\left(F_{\text{model-gamma}},\ F_{\text{plaque}}\right). \quad (10)$$

2) Discrete Fréchet Distance Feature Extracted From Piecewise Curves: In order to acquire more effective features, we extracted the DFDFs from the piecewise curves. The CDF of each plaque and the model curves were divided intp step lengths of 255, 50 or 30 gray levels, as shown in Table I.

3) Gray-Scale Median: The GSM of a carotid plaque is a common metric for evaluating plaque echogenicity. We measured the GSM of each plaque in this study. The effectiveness of GSM in identifying the echolucent plaques was investigated and compared with that of DFDFs.

TABLE I
THE SCHEME OF CURVE SEGMENTATION

Feature set	Step length	Gray level ranges of the piecewise curves	Number of features
1	255	0–255	3
2	50	0–50, 51–100, 101–150, 151–200, 201–255	15
3	30	0–30, 31–60, 61–90, 91–120, 121–150, 151–180, 181–210, 211–255	24

G. Feature Reduction and Classification

1) Linear Discriminant Analysis: Before classification, feature reduction was necessary to consider the relative large amount of DFDFs. Linear discriminant analysis (LDA) is a useful tool for pattern recognition [25]. It is widely used in process of feature reduction by providing a linear transformation of the feature space. Here, LDA was implemented for DFDFs and the most discriminating features (MDFs) were obtained.

Let DFDF_g^c denote the DFDF of the gth plaque in class c, and $c = 1, 2, 3$. Define the within-class scatter matrix S_W *as*

$$S_W = \frac{1}{\mathrm{N_{all}}}\sum_{c=1}^{c}\sum_{g=1}^{\mathrm{N}_c}(\mathrm{DFDF}_g^c - \upsilon_c)(\mathrm{DFDF}_g^c - \upsilon_c)^T \quad (11)$$

where υ_c is the mean vector of the cth class, $\mathrm{N_{all}}$ is the number of all the sample, $\mathrm{N_c}$ is the number of the sample in the cth class. Define the between classes scatter matrix S_B as

$$S_B = \frac{1}{\mathrm{N_{all}}}\sum_{c=1}^{c}\mathrm{N}_c(\upsilon_c - \upsilon)(\upsilon_c - \upsilon)^{\mathrm{T}} \quad (12)$$

where υ is the mean vector of the pooled data. The aim of LDA is to find a linear transform matrix ω such that the objective

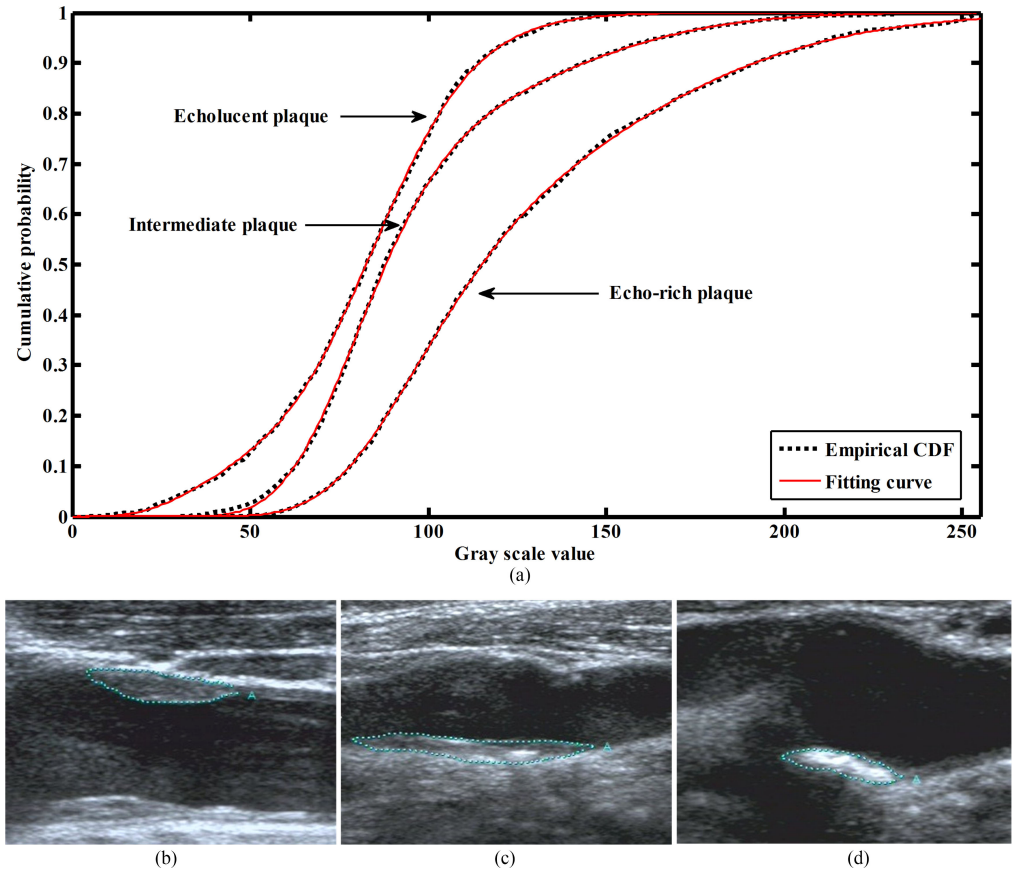

Fig. 2. Cumulative distribution function (CDF) of bimodal gamma distribution fitting empirical CDF of the gray value distributions of the plaques. The empirical CDFs in (a) was drew according to the echolucent, intermediate and echo-rich plaques defined in (b), (c) and (d), respectively. The parameters of fitting curve were $\beta = 0.31$, $k_1 = 4.44$, $\theta_1 = 13.79$, $k_2 = 20.49$, $\theta_2 = 4.44$, $\varepsilon = 0.0020$ (echolucent); $\beta = 0.19$, $k_1 = 21.93$, $\theta_1 = 6.69$, $k_2 = 19.54$, $\theta_2 = 4.32$, $\varepsilon = 0.0028$ (intermediate); $\beta = 0.42$, $k_1 = 13.84$, $\theta_1 = 11.76$, $k_2 = 20.23$, $\theta_2 = 4.94$, $\varepsilon = 0.0019$ (echo-rich).

TABLE II
VISUAL CLASSIFICATION OF 330 CAROTID PLAQUES BY TWO OBSERVERS

		First observer			
		Echo-rich	Intermediate	Echolucent	Total
Second observer	Echo-rich	106	2	1	109
	Intermediate	1	105	4	110
	Echolucent	0	0	111	111
	Total	107	107	116	330

$\kappa = 0.964$

function as maximizing the following:

$$J(\omega) = \underset{\omega}{\operatorname{argmax}} \frac{\left|\omega^{\mathrm{T}} S_B \omega\right|}{\left|\omega^{\mathrm{T}} S_W \omega\right|}. \tag{13}$$

It can be proved that such a transform Φ is composed of eigenvectors corresponding to largest eigenvalues of S_B S_W. The MDFs can be produced by the transformation:

$$\mathrm{MDFs} = \Phi^T \mathrm{DFDFs}. \tag{14}$$

2) K-Nearest-Neighbor (KNN) Classifier: In the KNN algorithm, a new input case is classified by a majority vote of its neighbors from the training set. In this study, the case is assigned to the most frequent class among its K nearest neighbors based on the Euclidean distance. The KNN carotid plaque classification system was implemented for the value of 3 and it was tested using for input the MDFs of feature sets 1–3 and GSM.

III. RESULTS

A. Visual Classification

The visual classification of the carotid plaques ($n = 330$) into three different types showed a good inter-agreement (see Table II). The inter-observer reproducibility was 97.57% ($\kappa = 0.964$). A total of eight controversial plaques were excluded, and the remaining 105 echo-rich, 105 intermediate and 105 echolucent consensual plaques were randomly selected for the following analysis.

B. Model Curves of Plaque Based on Bimodal Gamma Distribution

Fig. 2 shows that the CDF of bimodal gamma distribution is effective in fitting the empirical CDF of the echo-rich, intermediate and echolucent plaques. The statistical model of the gray value distribution of plaque was shown in Fig. 3. The CDF of bimodal gamma distribution with parameters ($\beta = 0.5$,

TABLE III
DISCRETE FRÉDCHET DISTANCE FEATURE SETS

		Echo-rich	Intermediate	Echolucent	F value	p value
Feature set 1	MDFs 1	1.07 ± 0.66	-0.24 ± 0.99	-0.84 ± 0.83	141.67	< 0.001
	MDFs 2	0.13 ± 1.12	-0.41 ± 0.77	0.29 ± 0.96	15.32	< 0.001
Feature set 2	MDFs 1	0.29 ± 0.14	-0.61 ± 0.21	-0.23 ± 0.15	254.44	< 0.001
	MDFs 2	-0.01 ± 0.04	0.04 ± 0.05	-0.02 ± 0.04	65.49	< 0.001
Feature set 3	MDFs 1	0.25 ± 0.12	-0.05 ± 0.17	-0.19 ± 0.13	274.04	< 0.001
	MDFs 2	-0.02 ± 0.06	0.06 ± 0.08	-0.04 ± 0.05	71.04	< 0.001

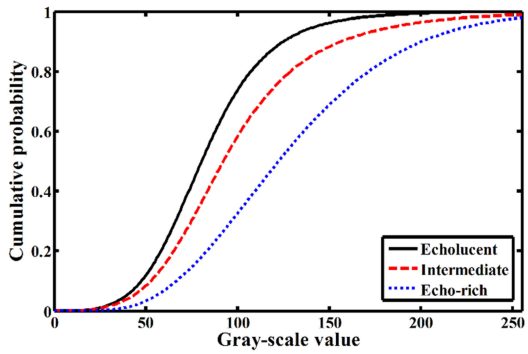

Fig. 3. Model curves of the three types of plaques based on bimodal gamma distribution. The parameters of CDF are $\beta = 0.5$, $k_1 = 4.74$, $\theta_1 = 18.19$, $k_2 = 13.14$, $\theta_2 = 6.34$ (echolucent); $\beta = 0.5$, $k_1 = 3.76$, $\theta_1 = 29.19$, $k_2 = 11.41$, $\theta_2 = 8.03$ (intermediate); $\beta = 0.5$, $k_1 = 6.73$, $\theta_1 = 15.27$, $k_2 = 9.51$, $\theta_2 = 16.48$ (echo-rich).

$k_1 = 4.74$, $\theta_1 = 18.19$, $k_2 = 13.14$, $\theta_2 = 6.34$), ($\beta = 0.5$, $k_1 = 3.76$, $\theta_1 = 29.19$, $k_2 = 11.41$, $\theta_2 = 8.03$) and ($\beta = 0.5$, $k_1 = 6.73$, $\theta_1 = 15.27$, $k_2 = 9.51$, $\theta_2 = 16.48$) represents the echolucent, intermediate and echo-rich plaques. The distance between the three model curves showed a trend of first increase and then decrease as gray value increasing (see Fig. 3). And the curve of echolucent plaque can be distinguished from the other two model curves.

C. Feature Extraction and Classification

For each plaque, a total of 42 DFDFs (feature set 1 with 3 features, feature set 2 with 15 features, and feature set 3 with 24 features) were obtained. LDA was performed for each feature set, and two MDFs (MDF1 and MDF2) were obtained. All MDF1 and MDF2 of feature set 1 to 3 were significantly different between the three types of plaques (all, $p < 0.001$) (see Table III). Fig. 4 illustrates the two-dimensional scatter-plots of 315 plaques using MDF1 and MDF2. The scattered point distributions based on MDFs obtained from feature set 2 and set 3 constituted three more distinct congregate areas compared with feature set 1. Accordingly, the classification accuracy of three types of plaques were 68.25%, 75.87% and 77.46% when using MDFs of feature set 1 to 3 for training.

D. Identification of Echolucent Plaques

Previous studies proved that echolucent plaques were potentially unstable and were regarded as high-risk plaques, whereas echo-rich and intermediate plaques were considered as low-risk [6], [8]. When echolucent plaques were identified using feature set 2, the accuracy, sensitivity and specificity were 85.09%, 77.14% and 89.04%, which were higher than these using feature set 1 (79.05%, 67.62% and 84.76%) and feature set 3 (83.17%, 75.24% and 88.09%) (see Table IV). Also the identification of echolucent plaques based on GSM showed a sensitivity of 72.38%, a specificity of 80.95% and a specificity of 63.33%. The receiver operating characteristic (ROC) is a standard method for assessing the sensitivity and specificity of diagnostic procedures, which provides a curve to describe the inherent tradeoff between the sensitivity and specificity of a diagnostic system. The ROC analysis was implemented to examine the ability of our method and GSM in identifying echolucent plaques. Fig. 5 shows the ROC curves for the KNN classifier when feature set 1 to 3 and GSM were used to train the classifier. The areas under the curve (AUC) for feature set 1-3 were 0.762, 0.831 and 0.812, which was higher than that for GSM (AUC = 0.712).

IV. DISCUSSION

In this study, a statistical model based on a bimodal gamma distribution was proposed to identify echo-rich, intermediate and echolucent plaques (see Fig. 3). Once the model was built, the problem of classification of plaques with different echogenicity was transformed into a mathematical problem for distinguishing similarity between the CDF of each plaque and the model curves, and the novel DFDFs were extracted for evaluating the similarity. The classification accuracy can reach 77.46%, when classifier was trained with the DFDFs. Furthermore, previous studies suggest that patients with echolucent plaques have a high risk of carotid bifurcation lesions [26] and ischemic cerebrovascular events [7]. Moreover, plaque echolucency is useful for predicting coronary events [3] and future strokes [9]. sFig. 5 shows that our method has a high potential for identifying echolucent plaques (AUC = 0.831). Therefore, a computer-aided method based on DFDFs may be promising in risk prediction of ACCEs for patients with plaques.

Visual identification is a common method for classification of plaques with different echogenicity [21], [27]–[29]. Mayor *et al.* visually classify 95 plaques into 5 types: type 1 (uniformly echolucent); type 2 (predominantly echolucent); type 3 (predominantly echogenic); type 4 (uniformly echogenic); and type 5 (unclassified plaques owing to calcification and producing acoustic shadows) [28] and they find that the plaques of type 1–5 presented intermediate mean GSMs, respectively of 33, 58, 100, 127 and 163, respectively. The mean GSM is linear related with the types (Spearman $r = 1$, $p < 0.05$),

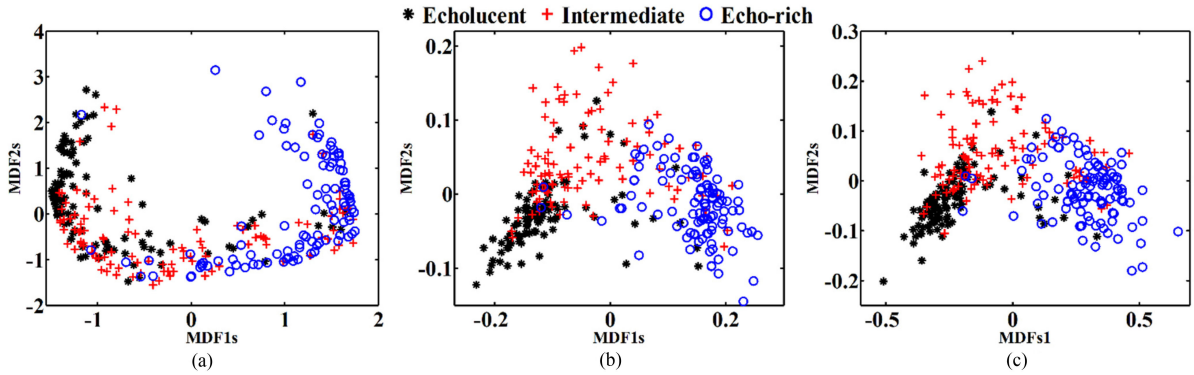

Fig. 4. Two-dimensional scatter-plots for 315 plaques using MDF1s and MDF2s. The MDFs in (a), (b), and (c) obtained from feature set 1, set 2 and set 3, respectively. MDF = most discriminating feature. Fig. 5. Receiver operating characteristic curves of identifying echolucent plaques for KNN classifier based on feature sets 1–3 and gray-scale median (GSM). AUC = area under the curve.

TABLE IV
RESULTS OF KNN CLASSIFICATION

	Accuracy				Sensitivity				Specificity			
	Feature set 1	Feature set 2	Feature set 3	GSM	Feature set 1	Feature set 2	Feature set 3	GSM	Feature set 1	Feature set 2	Feature set 3	GSM
Test 1	72.38%	84.78%	85.71%	67.62%	48.57%	71.43%	71.43%	82.86%	84.28%	91.42%	95.71%	60.00%
Test 2	78.10%	85.71%	77.14%	63.81%	77.14%	80%	74.29%	82.86%	78.57%	88.57%	78.57%	54.29%
Test 3	86.67%	84.78%	86.67%	85.71%	77.14%	80%	80%	77.14%	91.42%	87.14%	90%	75.71%
Average	79.05%	85.09%	83.17%	72.38%	67.62%	77.14%	75.24%	80.95%	84.76%	89.04%	88.09%	63.33%
Ranking	3	1	2	4	4	2	3	1	3	1	2	4

The three-fold cross validation in detailed. The accuracy, sensitivity and specificity of identifying echolucent plaques based on feature sets 1 to 3 and gray-scale median (GSM). The three-fold cross validation test included test 1 to 3.

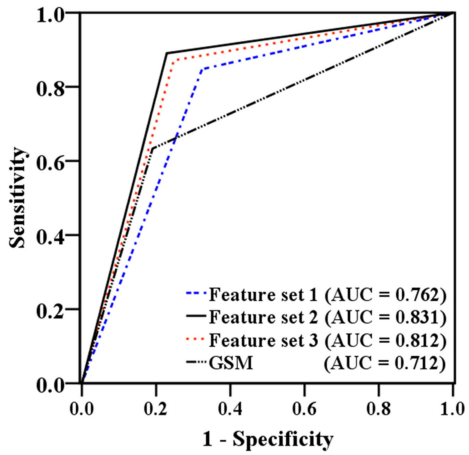

Fig. 5. Receiver operating characteristic curves of identifying echolucent plaques for KNN classifier based on feature sets 1–3 and gray-scale median (GSM). AUC = area under the curve.

and GSMs among different types of plaques show a statistical significance ($p < 0.02$). Plaques are classified visually into: type 1 (echo-rich), type 2 (intermediate) and type 3 (echolucent) in this study [21]. We compared the ability of DFDFs and GSM for identifying echolucent plaques. When the classifier was trained using MDFs of feature set2, the accuracy (85.09%) and the specificity (89.04%) were the highest, and a moderate sensitivity (77.14%) was achieved (see Table IV). The identification of echolucent plaques based on GSM showed a highest specificity of 80.95%, but it had a lower sensitivity (72.38%) and specificity (63.33%). Table IV shows the 3-fold cross validation analysis in detailed. Overall, the classification based on DFDFs feature set 2 had a higher stability than based on feature set 1, feature set 3 and GSM in identifying echolucent plaques.

In order to improve the comparability of the images acquired from different ultrasonic condition, images standardization is necessary before data processing. According to the method proposed by Elatrozy *et al.* [30], images were standardized manually by linearly adjusting the image so that the median gray level value of the blood was 0–5, and the median gray level value of the adventitia (artery wall) was 185-195. Moreover, Sabetai *et al.* have indicated that such an image normalization can decrease the variability between storage media and between probes [24]. In our study, all ultrasound images were normalized as the same as in [31]–[33].

In 1906, the Fréchet distance was defined as a measure of similarity between two parametric curves [34]. In 1994, Heikki *et al.* presented the discrete Fréchet distance, which is used for approximately computing Fréchet distance between two arbitrary curves using the discrete nodes along the curves for the measurements [35]. Many recent studies have proven the effectivity of discrete Fréchet distance [22], [23]. In this study, the most

discriminating features extracted from the DFDFs showed statistical difference between plaques with different echogenicity (see Table III). Furthermore, Irie *et al.* [36] in a study with 287 patients investigated the relationship between the echogenicity of carotid plaque and the occurrence of CVD events in detail. They divided the GSM values into quartiles (Q1: $\geq$ 59, Q2: 48-58, Q3: 38-47, and Q4: $\leq$ 37) and found that the lowest GSM quartile (Q4: GSM $\leq$ 37) has much higher risk for CVD as compare to the other GSM quartiles. Ruiz-Ares *et al.* [37] analyze 42 patients indicate that the unstable plaques have lower echogenicity than the stable plaques (GSM $=$ 23 vs. 37, $p < 0.001$). These studies suggest that plaque with different GSM had different level of risk, which may consistent with our results since more effective DFDFs can be obtained from the piecewise CDF of each plaque and the model curves in different gray level ranges.

The main limitation of present study is that the model curves were built with relatively few samples, and a more precise model is the next step for investigation. Moreover, we only took 255, 50 and 30 gray levels as step lengths to segment the curves, and DFDFs were extracted from piecewise curves. In order to obtain an optimal step length, the curve segmentation scheme needs detailed investigation. Our results may be verified with additional ultrasound images of carotid plaques.

V. Conclusion

Our results demonstrate the potential feasibility of the method for identifying echolucent plaques based on DFDFs, which may potentially improve the ability of noninvasive ultrasonic examination in risk prediction of ACCEs for patients with plaques.

References

[1] D. Mozaffarian *et al.*, "Heart disease and stroke statistics — 2016 update: A report from the American Heart Association," *Circulation*, vol. 133, no. 4, pp. e38–e360, 2016.

[2] R. J. Myerburg *et al.*, "Frequency of sudden cardiac death and profiles of risk," *Am. J. Cardiol.*, vol. 80, no. 5b, pp. 10f–19f, 1997.

[3] O. Honda *et al.*, "Echolucent carotid plaques predict future coronary events in patients with coronary artery disease," *J. Am. College Cardiol.*, vol. 43, no. 7, pp. 1177–1184, 2004.

[4] T. Nakamura *et al.*, "Ulcerated carotid plaques with ultrasonic echolucency are causatively associated with thromboembolic cerebrovascular events," *J. Stroke Cerebrovasc. Diseases*, vol. 22, no. 2, pp. 93–99, 2013.

[5] T. Nakamura *et al.*, "Ultrasound assessment of brachial endothelial vasomotor function in addition to carotid plaque echolucency for predicting cardiovascular events in patients with coronary artery disease," *Int. J. Cardiol.*, vol. 167, no. 2, pp. 555–560, 2013.

[6] M. L. M. Grønholdt *et al.*, "Lipid-rich carotid artery plaques appear echolucent on ultrasound B-mode images and may be associated with intraplaque haemorrhage," *Eur. J. Vasc. Endovasc. Surgery*, vol. 14, no. 6, pp. 439–445, 1997.

[7] E. B. Mathiesen *et al.*, "Echolucent plaques are associated with high risk of ischemic cerebrovascular events in carotid stenosis : The Tromso study," *Circulation*, vol. 103, no. 17, pp. 2171–2175, 2001.

[8] B. G. Nordestgaard *et al.*, "Echolucent rupture-prone plaques," *Current Opinion Lipidol*, vol. 14, no. 5, pp. 505–512, 2003.

[9] M. L. Gronholdt *et al.*, "Ultrasonic echolucent carotid plaques predict future strokes," *Circulation*, vol. 104, no. 1, pp. 68–73, 2001.

[10] L. Heng-Chao *et al.*, "An efficient and flexible statistical model based on generalized gamma distribution for amplitude SAR images," *IEEE Trans Geosci. Remote Sens.*, vol. 48, no. 6, pp. 2711–2722, Jul. 2010.

[11] X. Qin *et al.*, "Region-based classification of SAR images using Kullback-Leibler distance between generalized gamma distributions," *IEEE Geosci. Remote Sens.*, vol. 12, no. 8, pp. 1655–1659, Aug. 2015.

[12] A. Gumaei *et al.*, "Breast segmentation using k-means algorithm with a mixture of gamma distributions," in *Proc. Symp. Broadcast Netw. Fast Internet*, 2012, pp. 97–102.

[13] P. M. Shankar *et al.*, "Statistical modeling of atherosclerotic plaque in carotid B mode images—a feasibility study," *Ultrasound Med. Biol.*, vol. 29, no. 9, pp. 1305–1309, 2003.

[14] S. Nadarajah, "Statistical distributions of potential interest in ultrasound speckle analysis," *Phys. Med. Biol.*, vol. 52, no. 10, pp. N213–N227, 2007.

[15] Z. Tao *et al.*, "Evaluation of four probability distribution models for speckle in clinical cardiac ultrasound images," *IEEE Trans. Med. Imag.*, vol. 25, no. 11, pp. 1483–1491, Nov. 2006.

[16] G. Vegas-Sanchez-Ferrero *et al.*, "A generalized gamma mixture model for ultrasonic tissue characterization," *Comput. Math Methods Med.*, vol. 2012, pp. 1–25, 2012.

[17] G. Vegas-Sanchez-Ferrero *et al.*, "Gamma mixture classifier for plaque detection in intravascular ultrasonic images," *IEEE Trans. Ultrason. Ferroelectr. Freq. Control*, vol. 61, no. 1, pp. 44–61, Jan. 2014.

[18] A. El Zaart *et al.*, "Segmentation of SAR images," *Pattern Recog.*, vol. 35, no. 3, pp. 713–724, 2002.

[19] M. Petrou *et al.*, "Modelling the histograms of various classes in SAR images," *Pattern Recog. Lett.*, vol. 23, no. 9, pp. 1103–1107, 2002.

[20] M. Naghavi *et al.*, "From vulnerable plaque to vulnerable patient: A call for new definitions and risk assessment strategies: Part I," *Circulation*, vol. 108, no. 14, pp. 1664–1672, 2003.

[21] European carotid plaque study group, "Reprinted article "Carotid artery plaque composition–relationship to clinical presentation and ultrasound B-mode imaging," *Eur. J. Vasc. Endovasc. Surgery*, vol. 42, no. Suppl. 1, pp. S32–S38, 2011.

[22] J. Gudmundsson and N. Valladares, "A GPU approach to subtrajectory clustering using the Fréchet distance," *IEEE Trans Parallel Distrib. Syst.*, vol. 26, no. 4, pp. 924–937, Apr. 1, 2015.

[23] T. Wylie and B. Zhu, "Protein chain pair simplification under the discrete Fréchet distance," *IEEE/ACM Trans. Comput. Biol. Bioinformat.*, vol. 10, no. 6, pp. 1372–1383, Nov./Dec. 2013.

[24] M. M. Sabetai *et al.*, "Reproducibility of computer-quantified carotid plaque echogenicity: Can we overcome the subjectivity?," *Stroke*, vol. 31, no. 9, pp. 2189–2196, 2000.

[25] R. O. Duda *et al.*, *Pattern Classification*. New York, NY USA: Wiley, 2000.

[26] G. M. Biasi *et al.*, "Computer analysis of ultrasonic plaque echolucency in identifying high risk carotid bifurcation lesions," *Eur. J. Vasc. Endovasc. Surgery*, vol. 17, no. 6, pp. 476–479, 1999.

[27] G. Geroulakos *et al.*, "Characterization of symptomatic and asymptomatic carotid plaques using high-resolution real-time ultrasonography," *Brit. J. Surgery*, vol. 80, no. 10, pp. 1274–1277, 1993.

[28] I. Mayor *et al.*, "Carotid plaque: comparison between visual and grey-scale median analysis," *Ultrasound Med. Biol.*, vol. 29, no. 7, pp. 961–966, 2003.

[29] J. E. Wilhjelm *et al.*, "Quantitative analysis of ultrasound B-mode images of carotid atherosclerotic plaque: Correlation with visual classification and histological examination," *IEEE Trans. Med. Imag.*, vol. 17, no. 6, pp. 910–922, Dec. 1998.

[30] T. Elatrozy *et al.*, "The effect of B-mode ultrasonic image standardisation on the echodensity of symptomatic and asymptomatic carotid bifurcation plaques," *Int. Angiol.: A J. Int. Union Angiol.*, vol. 17, no. 3, pp. 179–186, 1998.

[31] C. I. Christodoulou *et al.*, "Texture-based classification of atherosclerotic carotid plaques," *IEEE Trans. Med. Imag.*, vol. 22, no. 7, pp. 902–912, Jul. 2003.

[32] D. A. Russell *et al.*, "Relationship of carotid plaque echomorphology to presenting symptom," *Eur. J. Vasc. Endovasc. Surgery*, vol. 39, no. 2, pp. 134–138, 2010.

[33] M. K. Salem *et al.*, "Identification of patients with a histologically unstable carotid plaque using ultrasonic plaque image analysis," *Eur. J. Vasc. Endovasc. Surgery*, vol. 48, no. 2, pp. 118–125, 2014.

[34] M. M. Fréchet, "Sur quelques points du calcul fonctionnel," *Rendiconti del Circolo Matematico di Palermo (1884-1940)*, vol. 22, no. 1, pp. 1–72, 2008.

[35] E. T. M. Heikki, "Computing discrete Fréchet distance," Tech. Rep. CD-TR 94/64, Inf. Syst. Dept., Tech. Univ. Vienna, *Vienna, Austria*, 1994.

[36] Y. Irie *et al.*, "The utility of ultrasonic tissue characterization of carotid plaque in the prediction of cardiovascular events in diabetic patients," *Atherosclerosis*, vol. 230, no. 2, pp. 399–405, 2013.

[37] G. Ruiz-Ares *et al.*, "A prediction model for unstable carotid atheromatous plaque in acute ischemic stroke patients: proposal and internal validation," *Ultrasound Med. Biol.*, vol. 40, no. 9, pp. 1958–1965, 2014.